Effective-medium approach to planar multilayer hyperbolic metamaterials: Strengths and limitations

Omar Kidwai, Sergei V. Zhukovsky, and J. E. Sipe
Department of Physics and Institute for Optical Sciences, University of Toronto, 60 St. George Street, Toronto, Ontario, Canada M5S 1A7
(Received 4 February 2012; published 31 May 2012)

We express the optical properties of multilayered hyperbolic metamaterials (HMMs) in terms of the Fresnel reflection coefficients at the boundary between the metamaterial and the ambient medium. Formation of a band of bulk propagating modes in HMMs located far outside the lightcone of homogeneous isotropic media is demonstrated. Exotic behavior of HMMs, such as the broadband Purcell effect and suppressed outward scattering, is reproduced. Conditions under which a metal-dielectric multilayer can be approximated by a homogeneous effective medium with extreme anisotropy (indefinite medium) are derived. It is shown that real multilayer HMMs usually have a smaller Purcell factor than the corresponding effective medium; however, the reverse scenario is shown to be possible due to an intermediary role of short-range surface plasmon excitations in the outermost metal layer in a metal-dielectric multilayer.

DOI: 10.1103/PhysRevA.85.053842 PACS number(s): 42.25.Bs, 78.67.Pt, 78.20.Ci, 42.50.Nn

I. INTRODUCTION

Metamaterials have attracted significant scientific interest because they offer a way to engineer optical materials with properties rare or absent in nature, such as media with negative refraction [1] or giant optical activity [2]. Other examples of such "exotic" optical properties are those exhibited by so-called "indefinite media," [3–6] which feature a special case of extreme anisotropy where diagonal elements of the permittivity tensor have different signs (e.g., $\epsilon_x = \epsilon_y < 0$, $\epsilon_z > 0$ for uniaxial anisotropic media). This causes the dispersion relation $\omega^2/c^2 = k_x^2/\epsilon_z + k_y^2/\epsilon_z + k_z^2/\epsilon_x$ to become hyperbolic rather than elliptical [see Figs. 1(a) and 1(b)]. In the idealization that such a dispersion relation holds for all wave vectors, the photonic density of states (DOS) becomes unbounded, giving rise to a variety of new physical phenomena including broadband spontaneous emission enhancement [7] and metric signature transitions [8]. Practical applications are also envisaged, such as highly absorptive coatings in which surface roughness is beneficial rather than detrimental [9].

Interest in indefinite media grew with the introduction of hyperbolic metamaterials (HMMs), which are metal-dielectric structures designed to approximately realize the dispersion relation of an indefinite medium [10]. An increase in the photonic DOS and the resulting physical effects were successfully confirmed in recent experiments [7,9–13]. As with other metamaterials, it is the subwavelength nature of the structuring that allows such metal-dielectric structures to be regarded as a homogeneous effective medium over a range of wave vectors. The two most straightforward implementations of HMMs are subwavelength metal-dielectric multilayers [7,9] and rod arrays [10,11,13,14]. For such geometries, the effective-medium approach is particularly simple. It involves averaging of permittivity in the directions tangential to the metal-dielectric boundaries (i.e., pointing along the rods or layer interfaces) and averaging of inverse permittivity in the directions normal to the metal-dielectric boundaries. For example, the structure in Fig. 1(c) with equal layer thicknesses corresponds to an effective medium with permittivity tensor components $\epsilon_x = \epsilon_y = (\epsilon_m + \epsilon_d)/2$ and $\epsilon_z^{-1} = (\epsilon_m^{-1} + \epsilon_d^{-1})/2$ (ϵ_m and ϵ_d are permittivities of metal and dielectric, respectively), resulting in the hyperbolic dispersion relation if $\epsilon_m < 0$ and $\epsilon_d > 0$. This simplicity makes the effective-medium approach very attractive to employ in theoretical calculations [7,11,14,15].

However, it is also evident that the range of applicability of effective-medium theory to such structures deserves investigation. While it is often mentioned that structural elements need to be "subwavelength," establishing such a condition must be done with care for extremely anisotropic metamaterials, because different polarizations of light behave very differently in the structure. HMMs, however, present even more difficulties because their salient properties rely on propagating waves with anomalously large wave vectors [7] and, hence, with anomalously short wavelength. This can cause the effective-medium approximation to break down far sooner than might be naively expected.

Indeed, our recent communication [16] confirms that, while the effective-medium approximation allows for the qualitative reproduction of the broadband Purcell effect for HMMs, the accuracy is rather poor for the layer thicknesses used in experiments to date, and effective-medium theory tends to overestimate the performance of actual HMMs. Another recent communication [17] reports that the effective-medium approximation can also underestimate the effects of multilayer HMMs on an emitter placed inside them. Very generally, the accuracy of the effective-medium theory was found to strongly depend on the details of the problem being studied, such as on the distance between a dipole emitter and an HMM structure [12,16], or the size of an emitter placed inside an HMM [18].

A physical understanding of the regime where one can rely upon the effective-medium approach in predicting the HMM properties is therefore important. It will necessarily rely on comparing the nature of wave propagation in a real HMM to that in the idealized indefinite medium resulting from homogenization and will lead to guidelines for the design of HMMs optimized for specific applications such as spontaneous emission control or suppression of back reflection. One approach to characterizing the behavior of metal-dielectric multilayers is based on the point spread function, which has been applied in a series of recent works

on subwavelength imaging [19–21]; however, its usefulness for the study of HMMs is still to be explored. Other strategies, such as a Green function approach [12] and cavity theory [17], have been applied. However, a systematic description of wave propagation in multilayer HMMs that would give insight into the emergence of a hyperbolic dispersion relation in metal-dielectric multilayers is still lacking.

In this paper we present a detailed calculation for the radiation rate of a dipole placed in close proximity to a generic metal-dielectric multilayer. Starting with the standard Green function approach [22,23] used in recent accounts [12,18], we describe multilayer HMMs based on the Fresnel reflection coefficients at the external boundary of the semi-infinite metamaterial. The expressions obtained for the radiation rate in terms of the Fresnel coefficients for propagating and evanescent waves with arbitrary wave vectors offer significant insight into the nature of wave propagation in HMMs and the coupling between an HMM and the outside environment. Such coupling between the evanescent near field of the dipole and propagating large wave vector modes in the HMM is confirmed as the reason for broadband spontaneous emission enhancement by HMMs. However, it turns out that the validity of the effective-medium approach for a particular multilayer HMM depends very strongly on the details of the problem considered. In particular, the layer thicknesses at which a real multilayer HMM functions as a homogeneous indefinite medium depend on the distance between the emitter and the metamaterial. We also identify the regimes where a multilayer structure can actually have better spontaneous emission enhancement than its homogenized effective-medium approximation, owing to an additional coupling via short-range surface plasmons in the outermost metal layer.

The rest of the paper is organized as follows: In Sec. II we outline the procedure to calculate the radiation of a dipole in close proximity to a generic multilayer, and apply it to HMM structures. In Sec. III we obtain and discuss Fresnel reflection coefficients for propagating and evanescent waves at the outer boundary of homogenized and actual HMMs. We establish the roles of bulk excitations in the HMM and surface excitations in the HMM's outermost layer. In the following Sec. IV we analyze the spontaneous emission enhancement for a dipole located close to ideal and real HMMs and arrive at applicability criteria for the effective-medium approximation. Finally, we summarize in Sec. V.

II. EMITTING DIPOLE NEAR MULTILAYER STRUCTURES

We consider an electric dipole $\boldsymbol{\mu}(t)$ a distance h above the top layer of a multilayer, at $\mathbf{r} = (0,0,h)$ [see Fig. 1(c)], embedded in a cladding of (real) refractive index n_c and oscillating at frequency ω:

$$\boldsymbol{\mu}(t) = \boldsymbol{\mu} e^{-i\omega t} + \text{c.c.} \tag{1}$$

We begin with a calculation of its rate of radiation into the cladding. The electric field is of the form

$$\mathbf{E}(\mathbf{r},t) = \mathbf{E}(\mathbf{r}) e^{-i\omega t} + \text{c.c.}, \tag{2}$$

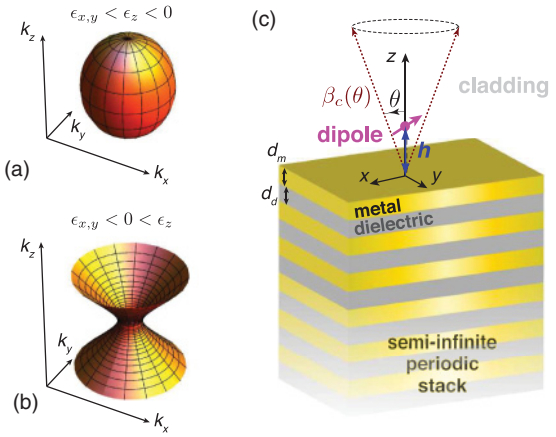

FIG. 1. (Color online) Schematic of isofrequency surface in dispersion relation $k_x^2/\epsilon_z + k_y^2/\epsilon_z + k_z^2/\epsilon_x = \omega^2/c^2$ for (a) conventional anisotropic medium ($\epsilon_x = \epsilon_y > 0, \epsilon_z > 0$) and (b) indefinite medium ($\epsilon_x = \epsilon_y < 0, \epsilon_z > 0$). (c) Semi-infinite multilayer HMM with average layer thickness $d = (d_m + d_d)/2$ studied in the present paper, with a dipole emitter close to its top surface.

and standard Green function techniques [22,23] can be employed to show that, for $z > h$, we have

$$\mathbf{E}(\mathbf{r}) = \frac{\tilde{\omega}^2}{4\pi\varepsilon_0} \int \frac{i d\boldsymbol{\kappa}}{2\pi w_c} [\mu_s(\boldsymbol{\kappa})\hat{\mathbf{s}} + \mu_p(\boldsymbol{\kappa})\hat{\mathbf{p}}_+] e^{i\boldsymbol{\kappa}\cdot\mathbf{R}} e^{i w_c z}, \tag{3}$$

where $\boldsymbol{\kappa}$ and $\mathbf{R}$ lie in the xy plane, $\mathbf{r} = \mathbf{R} + z\hat{\mathbf{z}}$,

$$\mu_s(\boldsymbol{\kappa}) = (e^{-i w_c h} + e^{i w_c h} R^s)\hat{\mathbf{s}} \cdot \boldsymbol{\mu},$$
$$\mu_p(\boldsymbol{\kappa}) = e^{-i w_c h} \hat{\mathbf{p}}_+ \cdot \boldsymbol{\mu} + e^{i w_c h} R^p \hat{\mathbf{p}}_- \cdot \boldsymbol{\mu},$$

and

$$w_c = \sqrt{\tilde{\omega}^2 n_c^2 - \kappa^2}, \tag{4}$$

with $\tilde{\omega} = \omega/c$; the square root of a complex number $\sqrt{z}$ is defined such that $\text{Im}\sqrt{z} \geqslant 0$ and, if $\text{Im}\sqrt{z} = 0$, $\text{Re}\sqrt{z} \geqslant 0$. Here $\hat{\mathbf{s}}$ and $\hat{\mathbf{p}}_\pm$ refer to the unit vectors in the direction of polarization for s- and p-polarized light, respectively, and in the latter case the signs in the subscript correspond to the vector for upward and downward propagating or evanescent waves,

$$\hat{\mathbf{s}} = \hat{\boldsymbol{\kappa}} \times \hat{z}, \quad \hat{\mathbf{p}}_\pm = \frac{\kappa\hat{\mathbf{z}} \mp w_c \hat{\boldsymbol{\kappa}}}{\tilde{\omega} n_c}.$$

The Fresnel coefficients R^s and R^p are those appropriate for light reflecting from the semi-infinite structure shown in Fig. 1. They depend on $\kappa = |\boldsymbol{\kappa}|, \tilde{\omega}, n_c$, the dielectric constants of metal and dielectric (ϵ_m, ϵ_d), and the thicknesses of metal layers (d_m) and dielectric layers (d_d) in the structure. We also introduce the average layer thickness d to mean

$$d = \frac{d_m + d_d}{2}. \tag{5}$$

An expression similar to Eq. (3) can be written for $\mathbf{H}(\mathbf{r})$, and as $r \to \infty$ the time-averaged Poynting vector reduces to

$$\mathbf{S}(\mathbf{r}) = 2\text{Re}[\mathbf{E}(\mathbf{r}) \times \mathbf{H}^*(\mathbf{r})]$$
$$= \frac{2 n_c c \epsilon_0 \tilde{\omega}^4}{(4\pi\epsilon_0)^2} \frac{|\mu_s(\boldsymbol{\kappa})|^2 + |\mu_p(\boldsymbol{\kappa})|^2}{r^2} \hat{\mathbf{r}}, \tag{6}$$

where the $\boldsymbol{\kappa}$ appearing on the right-hand side, and below, is the projection of $\tilde{\omega} n_c \hat{\mathbf{r}}$ onto the xy plane. Taking θ to be the angle defined in Fig. 1, and ϕ to be the angle between the projection of $\hat{\mathbf{r}}$ onto the xy plane and the $\hat{\mathbf{x}}$ axis, we look at the power radiated into a solid angle $d\Omega$ about $\hat{\mathbf{r}}$ and divide it by

$$W_{\rm ref} = \frac{2}{4\pi\epsilon_0}\frac{2}{3} c\tilde{\omega}^4 n_c \boldsymbol{\mu}^* \cdot \boldsymbol{\mu},$$

the total power radiated by a dipole embedded in a uniform medium of index n_c, to find

$$\lim_{r\to\infty} \frac{\mathbf{S}(\mathbf{r})\cdot\hat{\mathbf{r}} r^2}{W_{\rm ref}} = \frac{3}{8\pi\,(\boldsymbol{\mu}^*\cdot\boldsymbol{\mu})}[|\mu_s(\boldsymbol{\kappa})|^2 + |\mu_p(\boldsymbol{\kappa})|^2].$$

We refer to the integral of this over ϕ as $\beta^{\rm clad}(\theta)$ and find

$$\begin{aligned}\frac{4\beta^{\rm clad}(\theta)}{3} &= f_\perp^2 \frac{\kappa^2}{\tilde{\omega}^2 n_c^2}|1 + e^{2iw_c h} R^p|^2 \\ &\quad + \frac{1}{2} f_\parallel^2 \left[|1 + e^{2iw_c h} R^s|^2 + \frac{|w_c|^2}{\tilde{\omega}^2 n_c^2}|1 - e^{2iw_c h} R^p|^2\right],\end{aligned} \tag{7}$$

where $f_\perp^2 = |\boldsymbol{\mu}\cdot\hat{\mathbf{z}}|^2/(\boldsymbol{\mu}^*\cdot\boldsymbol{\mu})$ and $f_\parallel^2 = 1 - f_\perp^2$; $f_\parallel$ and $f_\perp$ are the normalized in-plane and out-of-plane components of the dipole moment [22]. The total radiation rate into the cladding, normalized by $W_{\rm ref}$, is then given by

$$b^{\rm clad} = \int_0^{\pi/2} \beta^{\rm clad}(\theta)\sin\theta d\theta = \frac{1}{\tilde{\omega} n_c}\int_0^{\tilde{\omega} n_c} \beta^{\rm clad}\frac{\kappa d\kappa}{w_c}, \tag{8}$$

with only the components lying inside the cladding's lightcone ($0 \leqslant \kappa \leqslant \tilde{\omega} n_c$) present in the field radiated into the cladding.

Besides the possibility to escape into the cladding, the energy radiated by the dipole can pass into the multilayer structure where, because of the absorption in the metallic layers, it will ultimately be absorbed. The total emission rate of the dipole b, normalized to $W_{\rm ref}$, will thus be greater than $b^{\rm clad}$. To find it, we calculate the work done by the dipole on the electromagnetic field. For the dipole at $\mathbf{r} = (0,0,h)$ the associated current density is $\mathbf{j}(\mathbf{r},t) = \mathbf{j}(\mathbf{r})\exp(-i\omega t) + \text{c.c.}$, where

$$\mathbf{j}(\mathbf{r}) = -i\omega\boldsymbol{\mu}\delta(\mathbf{R})\delta(z-h). \tag{9}$$

The rate at which work is done by a current distribution on the electromagnetic field is [24]

$$-\int \mathbf{j}(\mathbf{r},t)\cdot\mathbf{E}(\mathbf{r},t)dV,$$

and so the time-averaged total power radiated is

$$W = -2\text{Re}[\mathbf{j}^*(\mathbf{r})\cdot\mathbf{E}(\mathbf{r})] = 2\omega\text{Im}[\boldsymbol{\mu}^*\cdot\mathbf{E}(0,0,h)]. \tag{10}$$

Here the expression for the field, Eq. (2), is of the form [22,23]

$$\mathbf{E}(\mathbf{r}) = \mathbf{E}_S(\mathbf{r}) + \mathbf{E}_E(\mathbf{r}),$$

where $\mathbf{E}_S(\mathbf{r})$ is the field generated by a dipole in a uniform cladding, and

$$\mathbf{E}_E(\mathbf{r}) = \int \frac{i d\boldsymbol{\kappa}}{2\pi w_c}\frac{\tilde{\omega}^2}{4\pi\epsilon_0} e^{2iw_c h}[(R^s\hat{\mathbf{s}}\cdot\boldsymbol{\mu})\hat{\mathbf{s}} + (R^p\hat{\mathbf{p}}_-\cdot\boldsymbol{\mu})\hat{\mathbf{p}}_+] \tag{11}$$

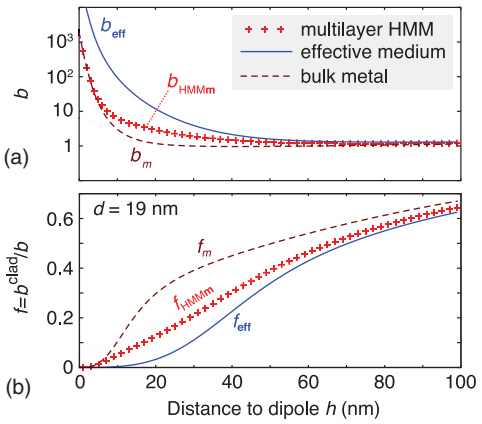

FIG. 2. (Color online) Dependence of (a) the total radiation rate b and (b) its fraction f directed into the cladding for an isotropically averaged dipole at a distance h above a multilayer HMM with metal as the top layer ("HMM**m**") and $d = 19$ nm as in Ref. [7], a homogenized effective medium given by Eq. (16), and a bulk metal. The material refractive indices are $\epsilon_m = -17.2 + 0.8i$ [27] and $\epsilon_d = 2.59$ [28] for $\lambda = 715$ nm, giving $\epsilon_x = \epsilon_y = -7.3 + 0.4i$ and $\epsilon_z = 6.1 + 0.05i$.

is the remaining contribution, associated with the reflection due to the multilayer. The result is

$$W = \frac{2}{4\pi\epsilon_0}\frac{2}{3} c\tilde{\omega}^4 n_c(\boldsymbol{\mu}\cdot\boldsymbol{\mu}^*) + 2\omega\text{Im}[\boldsymbol{\mu}^*\cdot\mathbf{E}_E(0,0,h)].$$

Dividing by $W_{\rm ref}$ and simplifying the resulting expression we finally obtain

$$\begin{aligned} b = 1 + \frac{3}{2\tilde{\omega} n_c}\text{Re}\Bigg(\int_0^\infty \frac{\kappa d\kappa}{w_c}\Bigg[f_\perp^2\frac{\kappa^2}{\tilde{\omega}^2 n_c^2}R^p \\ + \frac{1}{2}f_\parallel^2\left(R^s - \frac{w_c^2}{\tilde{\omega}^2 n_c^2}R^p\right)\Bigg]e^{2iw_c h}\Bigg).\end{aligned} \tag{12}$$

Numerical evaluation of this integral is unproblematic when absorption is present; the formal divergence at $w_c = 0$ can be removed by a change in variables, and the integral is finite for $h > 0$.

The classically calculated values of b and $b^{\rm clad}$ given by Eqs. (8) and (12) identify the normalized spontaneous emission rates that a quantum calculation would produce (see, e.g., Ref. [25]). Thus b has the meaning of a Purcell enhancement factor for spontaneous emission. The fraction of radiation escaping into the cladding, $f = b^{\rm clad}/b$, characterizes how good the structure is at suppressing reflected and backscattered radiation (i.e., how well it performs as a highly absorbing coating).

As an example demonstration of HMM properties, in Fig. 2 we show b and f for the structure in Jacob *et al.* [7], with $d_m = d_d = d = 19$ nm. We indicate the results for the calculation using the full multilayer by a subscript "HMM," the result using effective-medium theory by a subscript "eff," and the results for the replacement of the multilayer by solid metal by a subscript m; details of the calculations are presented in the next section. We see that both $b_{\rm eff}$ and $b_{\rm HMM}$ are much greater than b_m, confirming that an HMM affects the spontaneous emission rate much more strongly than bulk metal. The fraction of radiation directed into the cladding becomes drastically

suppressed by an HMM as compared to bulk metal [Fig. 2(b)]. This is in accordance with the results of previous theoretical and experimental works [7,9–13].

However, we notice that the discrepancy between the figures for effective-medium and a multilayer HMM is quite pronounced, and that b_{HMM} eventually approaches b_m as the dipole is brought close to the interface. Likewise, while f_{HMM} follows f_{eff} for larger h, it moves closer to f_m as h decreases. Therefore, the applicability of an effective medium approach with respect to HMMs warrants further investigation.

III. FRESNEL REFLECTION COEFFICIENTS

Equations (7) and (12) reveal that the structure influences the emission rate of the dipole placed next to it through the appearance of the Fresnel reflection coefficients $R^s = R^s(\kappa)$ and $R^p = R^p(\kappa)$ which will be the focus of this section.

It is important to note that, while Eq. (8) involves integration only within the lightcone in the cladding ($\kappa \leqslant \tilde{\omega} n_c$), Eq. (12) contains all possible values of κ, including waves that are either propagating or evanescent in the media involved. Since w_c is real for $\kappa < \tilde{\omega} n_c$ and purely imaginary ($w_c = iq_c$) for $\kappa > \tilde{\omega} n_c$ [see Eq. (4)], it is convenient to split the integral in Eq. (12) in the form

$$b = 1 + b_< + b_>, \tag{13}$$

where

$$b_< = \frac{3}{2\tilde{\omega} n_c}\mathrm{Re}\left(\int_0^{\tilde{\omega} n_c} \frac{\kappa\, d\kappa}{w_c}\left[f_\perp^2 \frac{\kappa^2}{\tilde{\omega}^2 n_c^2} R^p + \frac{1}{2} f_\parallel^2 \left(R^s - \frac{w_c^2}{\tilde{\omega}^2 n_c^2} R^p\right)\right] e^{2i w_c h}\right), \tag{14}$$

$$b_> = \frac{3}{2\tilde{\omega} n_c}\mathrm{Im}\left(\int_{\tilde{\omega} n_c}^{\infty} \frac{\kappa\, d\kappa}{q_c}\left[f_\perp^2 \frac{\kappa^2}{\tilde{\omega}^2 n_c^2} R^p + \frac{1}{2} f_\parallel^2 \left(R^s + \frac{q_c^2}{\tilde{\omega}^2 n_c^2} R^p\right)\right] e^{-2q_c h}\right). \tag{15}$$

Only the imaginary part of $R^s(\kappa)$ and $R^p(\kappa)$ for $\kappa > \tilde{\omega} n_c$ is seen to contribute to b. Thus, comparing $\mathrm{Im}R$ for the real multilayer HMM vs the homogenized effective medium will serve as a primary indication of how closely the effective medium reproduces the behavior of the real structure.

A. Homogenized effective medium

A multilayer with subwavelength layer thicknesses is conventionally homogenized using the Maxwell-Garnett formulas. The resulting effective medium is anisotropic and has the permittivity tensor $\epsilon = \mathrm{diag}(\epsilon_x, \epsilon_y, \epsilon_z)$ with the components

$$\epsilon_x = \epsilon_y = \rho\epsilon_m + (1-\rho)\epsilon_d, \tag{16}$$

$$\epsilon_z = \left[\rho\epsilon_m^{-1} + (1-\rho)\epsilon_d^{-1}\right]^{-1}, \tag{17}$$

where $\rho = d_m/(d_m + d_d)$ is the filling fraction of the metal. As an example, Fig. 3 shows the effective permittivity components ϵ_x and ϵ_z for gold-alumina multilayer structures similar to those used by Jacob *et al.* [7]. It can be seen that there is a broad region of filling fractions where $\mathrm{Re}\epsilon_x < 0$ and $\mathrm{Re}\epsilon_z > 0$,

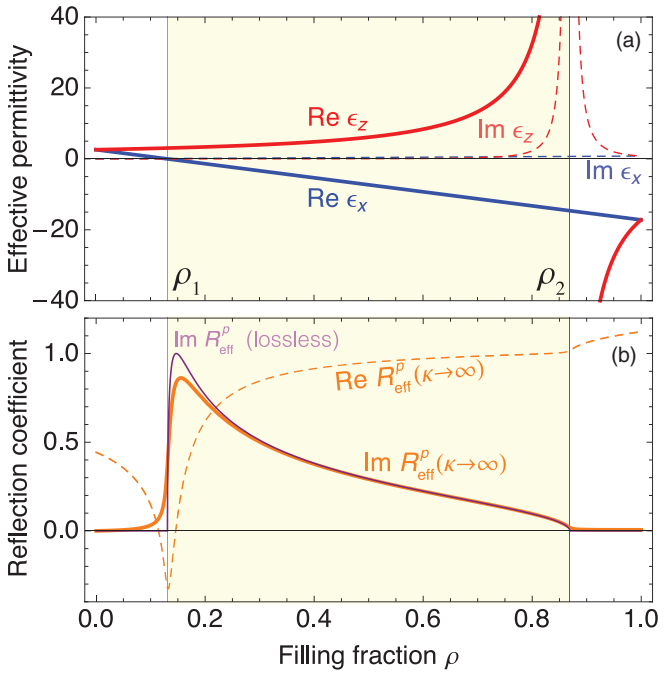

FIG. 3. (Color online) (a) Effective permittivities ϵ_x and ϵ_z for gold-alumina multilayers with different filling fraction ρ. The material refractive indices are $\epsilon_m = -17.2 + 0.8i$ [27] and $\epsilon_d = 2.59$ [28] for $\lambda = 715$ nm. (b) Asymptotic reflection coefficient $R^p_{\mathrm{eff}}(\kappa \to \infty)$ given by Eq. (22) for the same structures, with and without absorption losses. The shaded region denotes the range of $\rho \in [\rho_1; \rho_2]$ where the hyperbolic dispersion relation is exhibited.

so the effective medium is indeed indefinite. We define the boundaries of this region as ρ_1 and ρ_2, such that

$$\mathrm{Re}\epsilon_x(\rho_1) = 0, \quad [\mathrm{Re}\epsilon_z(\rho_2)]^{-1} = 0. \tag{18}$$

The Fresnel coefficients R^s_{eff} and R^p_{eff} at the interface between the cladding and such an effective medium are given by Ref. [23]

$$R^s_{\mathrm{eff}} = \frac{w_c - w^s_{\mathrm{eff}}}{w_c + w^s_{\mathrm{eff}}}, \quad R^p_{\mathrm{eff}} = \frac{w_c\epsilon_x - w^p_{\mathrm{eff}}\epsilon_c}{w_c\epsilon_x + w^p_{\mathrm{eff}}\epsilon_c}, \tag{19}$$

where w_c is given by Eq. (4), $\epsilon_c = n_c^2$, and

$$w^s_{\mathrm{eff}} = \sqrt{\tilde{\omega}^2\epsilon_x - \kappa^2}, \tag{20}$$

similar to an evanescent wave in a bulk metal; however,

$$w^p_{\mathrm{eff}} = \sqrt{\tilde{\omega}^2\epsilon_x - (\epsilon_x/\epsilon_z)\kappa^2}. \tag{21}$$

For very large κ, the second term under the square root in Eqs. (20) and (21) is dominant so that $w^s_{\mathrm{eff}} \approx w_c \approx i\kappa$, $w^p_{\mathrm{eff}} \approx \kappa\sqrt{-\epsilon_x/\epsilon_z}$. The reflection coefficients become independent of κ, approaching zero for s-polarized light [$R^s_{\mathrm{eff}}(\kappa \to \infty) = 0$] and a nonzero constant for p-polarized light:

$$R^p_{\mathrm{eff}}(\kappa \to \infty) = \frac{\epsilon_x - \sqrt{\epsilon_x/\epsilon_z}}{\epsilon_x + \sqrt{\epsilon_x/\epsilon_z}}. \tag{22}$$

If the metal were lossless and all permittivities were real, this asymptotic value of the reflection coefficient would be purely real unless the signs of ϵ_x and ϵ_z are different (i.e., everywhere except the HMM regime). Indeed, Fig. 3(b) shows

this for the gold-alumina multilayers. The presence of loss in the metal is seen to smear the abrupt appearance of nonzero $\mathrm{Im}R^p_{\mathrm{eff}}(\kappa\to\infty)$ at the HMM regime boundaries, with especially pronounced modification near ρ_1.

Regardless of whether losses are present or not, the emergence of an imaginary part in $R^p_{\mathrm{eff}}(\kappa\to\infty)$ makes $b_>$ in Eq. (15) diverge as h approaches zero, resulting in an unbounded enhancement of the spontaneous emission. This is indeed seen for $b_{\mathrm{eff}}(h)$ in Fig. 2(a).

B. Semi-infinite multilayers

We now compare the effective-medium reflection coefficients R^s_{eff} and R^p_{eff} with those of a semi-infinite metal-dielectric multilayer, R^s and R^p. For completeness, we consider two kinds of these multilayers with the topmost layer being either metal (labeled HMM**m**) or dielectric (HMM**d**). The expressions for R^s and R^p can be obtained by first constructing the transfer matrix for one period. For the HMM**m** structure it takes the form

$$M = M_m M_d = \begin{pmatrix} \frac{T_m^2-R_m^2}{T_m} & \frac{R_m}{T_m} \\ -\frac{R_m}{T_m} & \frac{1}{T_m} \end{pmatrix} \begin{pmatrix} \frac{T_d^2-R_d^2}{T_d} & \frac{R_d}{T_d} \\ -\frac{R_d}{T_d} & \frac{1}{T_d} \end{pmatrix}, \quad (23)$$

and the corresponding HMM**d** expression is written in the similar way as $M = M_d M_m$. The single-layer reflection and transmission coefficients in Eq. (23) are determined by the Airy formulas

$$T_j = \frac{\left(1-r_{cj}^2\right)\exp(i w_j d_j)}{1-r_{cj}^2\exp(2i w_j d_j)}, \quad (24)$$

$$R_j = \frac{r_{cj}[1-\exp(2i w_j d_j)]}{1-r_{cj}^2\exp(2i w_j d_j)}, \quad (25)$$

where $j = m, d$ and r_{cj} are the Fresnel reflection coefficients for the cladding-metal and cladding-dielectric interface, given by

$$r^s_{cj} = \frac{w_c - w_j}{w_c + w_j}, \quad r^p_{cj} = \frac{w_c\epsilon_j - w_j\epsilon_c}{w_c\epsilon_j + w_j\epsilon_c}, \quad j = m,d. \quad (26)$$

We can then insert infinitesimally thin layers of cladding material between each period in the structure [26]. The amplitudes of upward- and downward-propagating wave at the multilayer surface can be expressed as a column vector

$$\begin{pmatrix} R^s \\ 1 \end{pmatrix} \text{ or } \begin{pmatrix} R^p \\ 1 \end{pmatrix}$$

for the incident wave with amplitude equal to unity. Since removing one period from a semi-infinite periodic structure does not change it, the fields in the infinitesimal cladding layer below the topmost period

$$\begin{pmatrix} a^s_{\mathrm{up}} \\ a^s_{\mathrm{down}} \end{pmatrix}, \quad \begin{pmatrix} a^p_{\mathrm{up}} \\ a^p_{\mathrm{down}} \end{pmatrix} \quad (27)$$

should be proportional to the fields at the surface. From the transfer matrix relation

$$\begin{pmatrix} R^s \\ 1 \end{pmatrix} = M \begin{pmatrix} a^s_{\mathrm{up}} \\ a^s_{\mathrm{down}} \end{pmatrix}, \quad \begin{pmatrix} R^p \\ 1 \end{pmatrix} = M \begin{pmatrix} a^p_{\mathrm{up}} \\ a^p_{\mathrm{down}} \end{pmatrix}, \quad (28)$$

it thus follows that the vector in Eq. (27) should be an eigenvector of M. Of its two eigenvalues λ^s_1 and λ^s_2 (or λ^p_1 and λ^p_2), there should always be one with $|\lambda|>1$ as long as there is some absorption present in the period. From its corresponding eigenvector [Eq. (27)], one can obtain [26]

$$R^s = \frac{a^s_{0,\mathrm{up}}}{a^s_{0,\mathrm{down}}}, \quad R^p = \frac{a^p_{0,\mathrm{up}}}{a^p_{0,\mathrm{down}}}. \quad (29)$$

Figures 4 and 5 show the Fresnel reflection coefficients $R^s_{\mathrm{HMM\mathbf{m},d}}$ and $R^p_{\mathrm{HMM\mathbf{m},d}}$ for s- and p-polarized waves, respectively, under the same conditions as in Fig. 2 for both structures HMM**m** and HMM**d**.

For s-polarization, the wave that is transmitted into anisotropic HMM is ordinary. The normal component of its wave vector w^s_{eff} given by Eq. (20) is close to being purely imaginary for all κ, so R^s resembles the reflection coefficients for a dielectric-metal interface. Hence $|R^s| \lesssim 1$ for incident propagating waves with $\kappa < n_c\tilde{\omega}$ ($|R^s| = 1$ in the lossless limit), and $|R^s| < 1$ for the waves with $\kappa > n_c\tilde{\omega}$, which are evanescent both in the cladding and in the HMM medium. For the chosen values of $d_m = d_d = d = 12$ and 6 nm, the coefficients for real multilayers R^s agree well with R^s_{eff} (Fig. 4). It can be noticed that R^s_{eff} is between $R^s_{\mathrm{HMM\mathbf{m}}}$ and $R^s_{\mathrm{HMM\mathbf{d}}}$, which not surprisingly converge together as d decreases.

For p-polarization, the wave that is transmitted into the HMM is extraordinary and is characterized by hyperbolic dispersion relation. The coefficient $R^p(\kappa)$ behaves in a more complicated way, dictated by the the normal component of the wave vector w^p_{eff} as given by Eq. (21) [23]. For smaller κ, w^p_{eff} is close to being purely imaginary, and the behavior of R^p is similar to that of R^s (see Fig. 5) with the exception that it features a pole slightly outside the cladding lightcone at $\mathrm{Re}\kappa \gtrsim n_c\tilde{\omega}$. This pole corresponds to a surface plasmon polariton (SPP) excitation typical for a p-polarized wave at a dielectric-metal interface. Here, too, $R^p_{\mathrm{HMM\mathbf{m}}}$ and $R^p_{\mathrm{HMM\mathbf{d}}}$ approach R^p_{eff} from different sides and converge together as $d\to 0$.

As κ exceeds the critical value κ_{cr} given by $\kappa_{\mathrm{cr}}/\tilde{\omega} = \mathrm{Re}\sqrt{\epsilon_z}$, in our case equal to 2.467, the real part of the expression under the square root in Eq. (21) changes sign because $\mathrm{Re}(\epsilon_x/\epsilon_z) < 0$. Hence w^p_{eff} acquires a significant real part, signaling the *propagation* of transmitted fields in the HMM, while the reflected fields are strongly evanescent. From Eq. (19) we see that as this occurs when κ crosses κ_{cr}, there is a change of behavior in $R^p(\kappa)$ with an abrupt emergence of nonzero $\mathrm{Im}R^p$ (Fig. 5). As seen in Eq. (15), this leads to an increase of $b_>$ and, in turn, of the total emission rate b. However, unlike what we observed for s-polarized light and for p-polarized light with $\kappa < \kappa_{\mathrm{cr}}$, we now see a drastic difference between the effective medium and the real multilayer metamaterial structures. While R^p_{eff} stays essentially constant with increasing κ, as dictated by the asymptotic behavior in Eq. (22), both $\mathrm{Im}R^p_{\mathrm{HMM\mathbf{m}}}$ and $\mathrm{Im}R^p_{\mathrm{HMM\mathbf{d}}}$ initially follow $\mathrm{Im}R^p_{\mathrm{eff}}$ quite accurately but then drop off and decay toward zero.

It can also be noticed that while $\mathrm{Im}R^p_{\mathrm{HMM\mathbf{d}}}$ is less than $\mathrm{Im}R^p_{\mathrm{eff}}$ for all $\kappa > \kappa_{\mathrm{cr}}$, $\mathrm{Im}R^p_{\mathrm{HMM\mathbf{m}}}$ can exceed $\mathrm{Im}R^p_{\mathrm{eff}}$ in a certain range of κ. This "overshoot" effect becomes more pronounced if ρ decreases, and for $\rho \gtrsim \rho_1$ it becomes so drastic that the reflection coefficient for the real multilayer greatly differs from its effective-medium counterpart and becomes very strongly

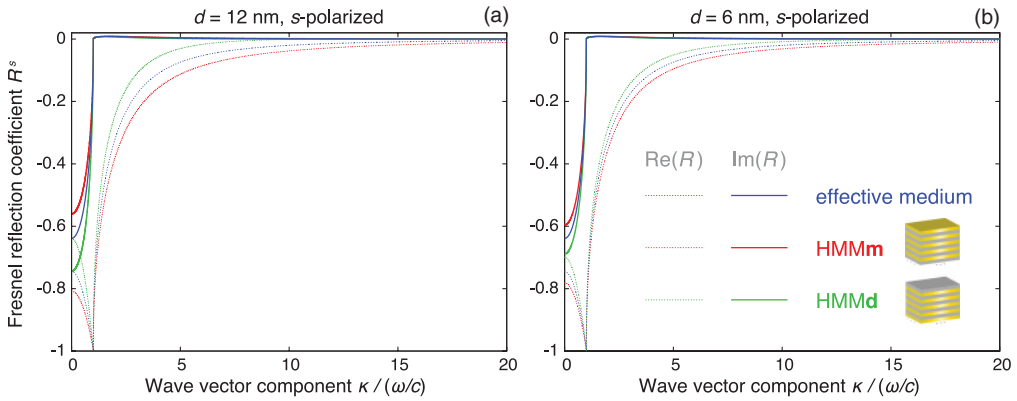

FIG. 4. (Color online) Fresnel reflection coefficient R^s for the effective medium and the multilayer HMM for (a) $d = 12$ nm and (b) $d = 6$ nm for s-polarized light, depending on tangential wave-vector component κ. The permittivities of metal and dielectric are the same as in Fig. 3, with $\rho = 0.5$.

dependent on whether the topmost layer is metal or dielectric (Fig. 6). It is also shown that the range of κ with nonzero $\mathrm{Im}R^p$ has clearly defined edges for a lossless metal. These edges are smeared in the presence of losses in a manner similar to what is seen in Fig. 3(b).

To summarize, we see that a contribution to the radiation rate b in Eq. (15) due to the nonzero imaginary part of R^p depends on (i) the asymptotic value of R^p_{eff} that R^p follows, (ii) the range of κ over which $\mathrm{Im}R^p \neq 0$, and (iii) the discrepancies between $\mathrm{Im}R^p_{\mathbf{HMMm}}$ (and $\mathrm{Im}R^p_{\mathbf{HMMd}}$) and $\mathrm{Im}R^p_{\mathrm{eff}}$ caused by the choice of the topmost layer. The first of these three is given by Eq. (22) so, for example, Fig. 3(b) reveals that $\rho \gtrsim \rho_1$ is an optimal choice of filling fraction if $\mathrm{Im}R^p$ needs to be maximized [see Eq. (18)]. The remaining two effects will be addressed in what follows.

C. Band formation for high-κ propagating modes

Having understood that nonzero $\mathrm{Im}R^p$ in a certain range of κ is associated with the existence of propagating high-κ modes in the HMM, we are now in position to determine that range in the case where it is clearly defined; namely, in the limit of *lossless* periodic metal-dielectric multilayers (see the insets in Fig. 6) where ϵ_m is taken to be real. From the Bloch theorem, it is known that the existence condition for propagating waves in a one-dimensional periodic medium is directly related to the properties of the one-period transfer matrix in Eq. (23) as [29,30]

$$-1 \leqslant \cos\left[k_B(d_m + d_d)\right] = \frac{\mathrm{Tr}M}{2} \leqslant 1, \tag{30}$$

where k_B is the z component of the wave vector for a Bloch wave. If the condition of Eq. (30) is not met, the structure does not support propagating Bloch waves and exhibits a photonic band gap. We are going to apply this condition to HMMs, substituting Eqs. (24) and (25) into Eq. (23). After some algebra, we see that

$$\frac{\mathrm{Tr}M}{2} = \cos\left[k_B(d_m + d_d)\right] = \cos(w_m d_m)\cos(w_d d_d) - \frac{1}{2}\left(\frac{\epsilon_m w_d}{\epsilon_d w_m} + \frac{\epsilon_d w_m}{\epsilon_m w_d}\right)\sin(w_m d_m)\sin(w_d d_d). \tag{31}$$

If the layer thicknesses are subwavelength and κ is not too large, it is expected that $w_j d_j \ll \pi$. Expanding Eq. (31) to the second order, we get

$$\frac{\mathrm{Tr}M}{2} \approx 1 - \frac{w_m^2 d_m^2}{2} - \frac{w_d^2 d_d^2}{2} - \left(\epsilon_m^2 w_d^2 + \epsilon_d^2 w_m^2\right)\frac{d_m d_d}{2\epsilon_m \epsilon_d}. \tag{32}$$

This equals unity at

$$\kappa_{\mathrm{lower}} = \tilde{\omega}\sqrt{\left[\frac{d_m \epsilon_m^{-1}}{d_m + d_d} + \frac{d_d \epsilon_d^{-1}}{d_m + d_d}\right]^{-1}} = \tilde{\omega}\sqrt{\epsilon_z}, \tag{33}$$

which coincides with κ_{cr} from the previous section. Thus, the lower band edge for the high-κ propagating modes in the HMM is indeed determined by the value of κ where the eigenwaves in the homogenized effective medium change from evanescent to propagating. The lower band edge is correctly predicted by the effective-medium approach as long as the phase variation across each layer $w_j d_j$ ($j = m, d$) is sufficiently small at $\kappa = \kappa_{\mathrm{cr}}$ to allow Eq. (31) to be expanded. Unless ϵ_z is very large [i.e., for ρ not too close to ρ_2; see Fig. 3(a)], $w_j(\kappa_{\mathrm{cr}})$ is on the order of $\tilde{\omega}\sqrt{\epsilon_j}$, so the conventional subwavelength criterion $n_j d_j \ll \lambda$ holds here. This can be confirmed in Fig. 7(a) where Eq. (33) is seen to give an accurate prediction for κ_{lower} for layer thicknesses of up to 50 nm unless the filling fraction approaches ρ_2 where $1/\epsilon_z = 0$.

More generally, if the left-hand side of Eq. (32) is expanded as $1 - k_B^2(d_m + d_d)^2/2$, the resulting expression

$$k_B^2(d_m + d_d)^2 = w_m^2 d_m^2 + w_d^2 d_d^2 + \left(\epsilon_m^2 w_d^2 + \epsilon_d^2 w_m^2\right)\frac{d_m d_d}{\epsilon_m \epsilon_d} \tag{34}$$

reduces to

$$\frac{\omega^2}{c^2} = \frac{k_B^2}{\epsilon_x} + \frac{\kappa^2}{\epsilon_z}, \tag{35}$$

in full accordance with the predictions of the effective-medium theory. Hence we can conclude that hyperbolic dispersion relation in periodic HMMs originates from the dispersion relation for Bloch waves with high κ in the approximation that $d_{m,d}(\tilde{\omega}^2\epsilon_{m,d} - \kappa^2)^{1/2} \ll \pi$. Following the standard reasoning

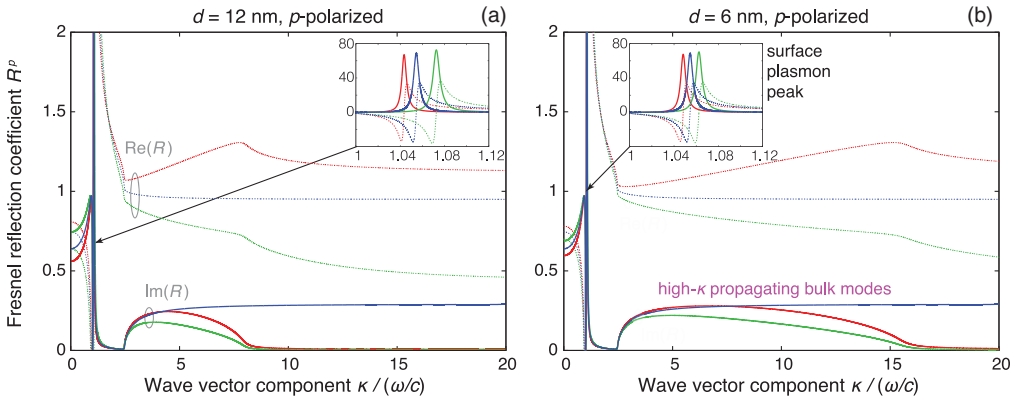

FIG. 5. (Color online) Same as Fig. 4 but for p-polarized light. The insets show an enlarged view of long-range SPP peak for $\kappa \gtrsim \tilde{\omega}$.

for wave propagation in periodic media, these Bloch waves result from coupling between excitations in individual structure period [29]. Out of all possible excitations, the short-range SPP (SRSPP) in thin-layer metal-dielectric structures have a very high κ and should therefore be associated with Bloch wave formation. The role of these SRSPPs in the appearance of propagating waves in metal-dielectric multilayers was discussed by Rosenblatt and Orenstein [30].

The upper band edge occurs at a large κ, which we label κ_{upper}, where $w_{m,d} = iq_{m,d}$ are purely imaginary and have a large magnitude, so the expansion to any finite order of $w_j d_j$ cannot be made. Here it is convenient to rewrite Eq. (31) in the form

$$\frac{\text{Tr}M}{2} = \frac{1}{4}(1+\eta)[e^{q_m d_m + q_d d_d} + e^{-(q_m d_m + q_d d_d)}] + \frac{1}{4}(1-\eta)[e^{q_m d_m - q_d d_d} + e^{q_d d_d - q_m d_m}], \quad (36)$$

where

$$\eta = \frac{1}{2}\left(\frac{\epsilon_m q_d}{\epsilon_d q_m} + \frac{\epsilon_d q_m}{\epsilon_m q_d}\right). \quad (37)$$

For large κ so that $q_{m,d} \approx \kappa$, η becomes independent of κ,

$$\eta \to \frac{1}{2}\left(\frac{\epsilon_m}{\epsilon_d} + \frac{\epsilon_d}{\epsilon_m}\right). \quad (38)$$

Note that the right-hand side of Eq. (38) is less than -1 because $\epsilon_m < 0$. So the dominant exponent $e^{q_m d_m + q_d d_d}$ in Eq. (36) has a negative prefactor and the whole expression will eventually approach negative infinity:

$$\lim_{\kappa\to\infty} \frac{\text{Tr}M}{2} = -\infty.$$

Since $(\text{Tr}M)/2 = 1$ at κ_{lower} [see Eqs. (31) and (32)], there should be a certain $\kappa_{\text{upper}} > \kappa_{\text{lower}}$ where $(\text{Tr}M)/2 = -1$, and this value will be the upper band edge for the high-κ modes.

In the particular case of $d_m = d_d = d$ ($\rho = 0.5$), which is experimentally relevant [7], the expression in brackets on the second line of Eq. (36) reduces to 2. For sufficiently large κ so that the expression in Eq. (38) can be used for η, Eq. (36) becomes

$$\frac{\text{Tr}M}{2} \approx \frac{1}{4}(1+\eta)e^{2\kappa d} + \frac{1}{2}(1-\eta),$$

and κ_{upper} can be analytically determined as

$$\kappa_{\text{upper}} = \frac{1}{2d}\ln\left[\frac{2(\eta-3)}{\eta+1}\right]. \quad (39)$$

This agrees with the arguments of Jacob *et al.* [7] where it was speculated that the cutoff wave number for the high-κ modes should scale as d^{-1}. For a different filling fraction, it can be seen that the second term of Eq. (36) is positive and increases the total expression, so κ_{upper} should increase compared to its value for $\rho = 0.5$. This is indeed seen in Fig. 7(b). One can also see that Eq. (39) remains valid for periods over a wide range, extending to greater than 50 nm.

The reason why the reflection coefficient of multilayer HMMs eventually departs from that of the effective medium is that the condition $w_{m,d}d \ll 1$ inevitably becomes violated for larger κ, no matter how small d is. In other words, high-κ propagating modes have a much shorter wavelength at a given ω than the vacuum wavelength $2\pi c/\omega$, and it is against this shortened wavelength that the layer thickness d should be compared. Hence the effective-medium approximation *always* breaks down in HMMs for p-polarization: for any given layer thickness d there exists a $\kappa < \kappa_{\text{upper}}$ for which $w_{m,d}(\kappa)d \ll 1$ fails, and $R^p \neq R^p_{\text{eff}}$. Even in the case of naturally occurring homogeneous indefinite media (such anisotropy is observed in some polaritonic crystals [8] or graphite [31]), d has the meaning of interatomic distances, on the order of 0.1 nm. So there will still exist a value of κ beyond which the propagating modes will no longer be supported.

D. Influence of topmost layer

Using the Bloch theorem to derive the dispersion properties of a metal-dielectric multilayer implies that the structure is infinite. In a semi-infinite structure such as shown in Fig. 1(c), the topmost layer (metal or dielectric) is special because it is adjacent to the cladding. This effect can be noticed in Figs. 4 and 5 where the reflection coefficients for HMM**m** and HMM**d** structures are seen to be slightly different. In fact, this difference can become so great (see Fig. 6) that the choice of the topmost layer can be assumed to dominate the behavior of the Fresnel coefficient in a wide range of κ. This assumption can be verified by showing that putting a single metal or dielectric layer on top of a homogenized effective medium

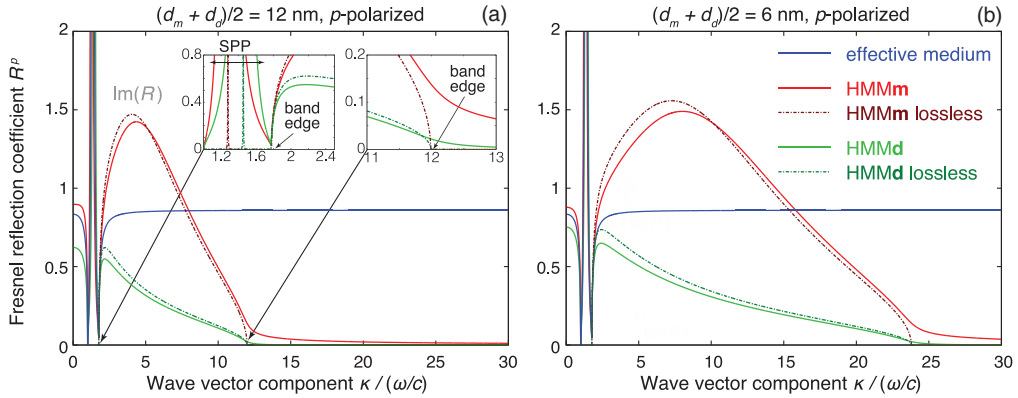

FIG. 6. (Color online) Same as Fig. 5 but for a smaller filling fraction of $\rho = 0.156$. Dash-dotted lines correspond to the case when losses in the metal are neglected. The insets show enlarged views near the edges of high-κ bulk propagating mode band.

reproduces the variation between the reflection coefficients of HMM**m** vs HMM**d** relatively faithfully [Fig. 8(a)].

Hence the reflection of, for example, HMM**m** can be approximated by a generalized Airy formula [32]

$$R^p_{\mathrm{HMM}\mathbf{m}} \approx \frac{R_m + R^p_{\mathrm{eff}}\left(T_m^2 - R_m^2\right)}{1 - R^p_{\mathrm{eff}} R_m}, \tag{40}$$

where R_m and T_m are single-layer coefficients given by Eqs. (24) and (25), and R^p_{eff} is the effective-medium coefficient from Eq. (19).

It is known that a thin metal layer supports SPP excitations for p-polarized light, and that their wave vectors are determined by poles in R_m or by zeros in the denominator in Eq. (25):

$$1 - r_{cm}^2 \exp(2i w_m d_m) = 0. \tag{41}$$

One such pole corresponds to $\kappa \gtrsim \tilde{\omega} n_c$ and can be determined by an assumption that $\kappa \approx \tilde{\omega} n_c$ everywhere except in w_c. This pole is a symmetric coupling between SPPs at the cladding-metal interface and is called the long-range SPP (see, e.g., the review by Berini [33] and references therein). The other pole, arising from antisymmetric coupling between interface SPPs, has a much larger κ and is therefore of primary importance to HMMs. It is called the short-range SPP (SRSPP). It can be determined by assuming that κ is sufficiently large in Eq. (41), so that $w_m \approx i\kappa$ and $r_{cm} \approx r_{cm}^{\mathrm{lim}} \equiv (\epsilon_m - \epsilon_c)/(\epsilon_m + \epsilon_c)$ is a constant. The pole location is then given by

$$\kappa_{sp} \approx \mathrm{Re}\frac{\ln r_{cm}^{\mathrm{lim}}}{d_m}, \tag{42}$$

which is within 10% of the actual value for layers up to 5 nm thick, and which makes a good initial guess if Eq. (41) needs to be numerically solved for κ_{sp}. Then, one can expand R_m and T_m in the vicinity of κ_{sp} according to Ref. [34]

$$R_m = \frac{\rho_m}{\kappa - \kappa_{sp}}, \quad T_m^2 - R_m^2 = \frac{\delta_m}{\kappa - \kappa_{sp}}, \tag{43}$$

where, in the same approximation as Eq. (42),

$$\rho_m \approx \frac{r_{cm}^{\mathrm{lim}} - 1/r_{cm}^{\mathrm{lim}}}{2d_m}, \quad \delta_m \approx -2\rho_m. \tag{44}$$

With Eq. (43) and R^p_{eff} approximated by Eq. (22), Eq. (40) becomes

$$R^p_{\mathrm{HMM}\mathbf{m}} \approx \frac{\rho_m + \delta_m R^p_{\mathrm{eff}}}{\kappa - \kappa_{sp} - \rho_m R^p_{\mathrm{eff}}}, \tag{45}$$

which has a better correspondence to Eq. (40) than the effective-medium approximation [see Fig. 8 (b)].

We see that, besides a shift in the SRSPP pole, which is expected whenever the medium next to a metal layer is changed, an imaginary part of R^p_{eff} causes the SRSPP resonance

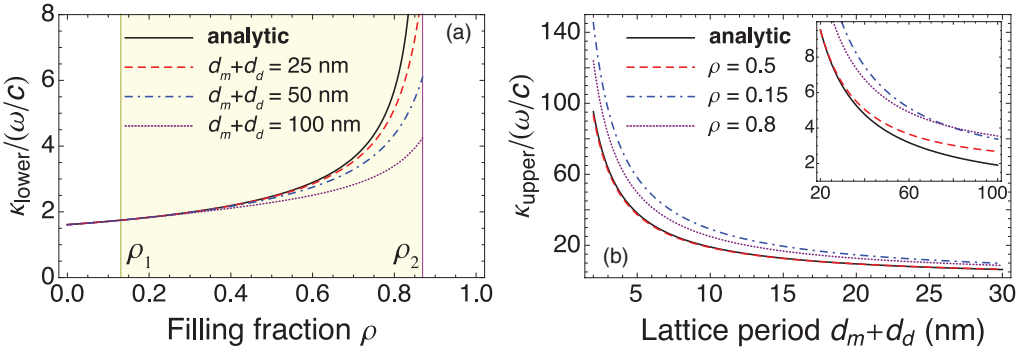

FIG. 7. (Color online) (a) Comparison between lower HMM band edge κ_{lower} obtained by Eq. (33) and directly from Eq. (31) for period $d_m + d_d = 25, 50, 100$ nm. (b) Comparison between the upper HMM band edge κ_{upper} obtained from Eq. (39) and directly from Eq. (36) for the filling fraction $\rho = 0.15, 0.5, 0.8$. The inset shows an extended view for the period up to 100 nm.

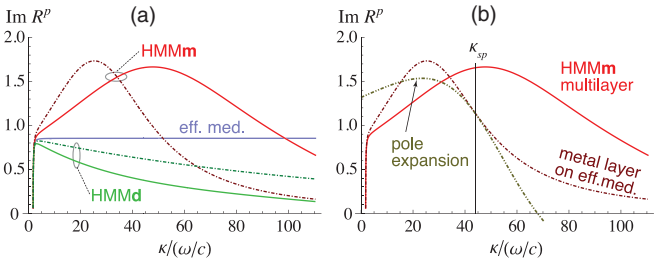

FIG. 8. (Color online) Comparison between imaginary part of $R^p(\kappa > \kappa_{cr})$ (a) for effective medium, actual multilayer HMM**m** and HMM**d** (solid lines), and approximations formed by placing a single metal or dielectric layer atop the effective medium [Eq. (40), dash-dotted lines] and (b) for the actual multilayer HMM**m** (solid), the approximation of Eq. (40) (dash dot), and the pole expansion of Eq. (45) (dash dot dot) for $\rho = 0.15$ and $d_m + d_d = 2$ nm.

to broaden even without material losses due to the interaction between the SPP mode and the propagating modes in an HMM. Such a broadened SRSPP excitation encompasses a wider range of wave vectors than an SRSPP in an isolated metal layer, which can only be broadened due to the action of losses in metal. Thus, an SRSPP in a metal layer between the cladding and the HMM can couple to evanescent field in the cladding more strongly. Such an SRSPP acts as an intermediary between the dipole field and the propagating modes in the HMM, which is signified by the increase in the imaginary part of the reflection coefficient compared to the results of the effective-medium approximation.

Unfortunately, the shifted SRSPP pole κ_{max} may lie far outside the immediate vicinity of κ_{sp} [i.e., outside the range of validity of the expansion in Eq. (43)]. However, a numerical estimate of the coupling enhancement can still be given by computing the value of $\mathrm{Im}R^P_{\mathrm{HMMm}}(\kappa_{\max})$ depending on the filling fraction. The results (see Fig. 9) show that the strongest enhancement occurs in the vicinity of ρ_1, and that material absorption in the metal further increases $\mathrm{Im}R^p_{\mathrm{HMMm}}(\kappa_{\max})$. This is because losses in metal broaden the SRSPP even more and produce an additional dissipation channel for the external field in the cladding. While this effect is rather detrimental if high-κ propagating modes are used (e.g., for subwavelength imaging purposes), it can be beneficial for designing scattering-free coatings and cloaks [9].

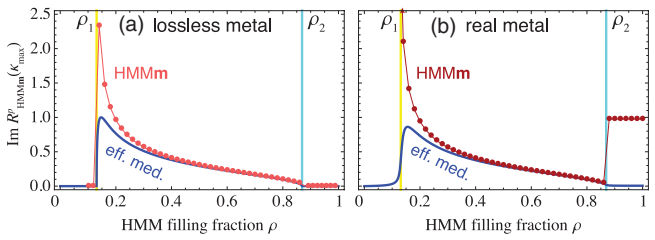

FIG. 9. (Color online) Im $R^p_{\mathrm{HMMm}}(\kappa = \kappa_{\max})$ depending on ρ (dots) vs Im R^p_{eff} (solid blue line) for (a) lossless metal and (b) real gold. The vertical lines denote the bounds of HMM region.

IV. SPONTANEOUS EMISSION ENHANCEMENT

We now return to Eqs. (7), (8), and (12)–(15) to quantify how the radiation properties of a dipole are modified in the immediate vicinity of a HMM vs a homogenized effective medium. The first thing to notice is that the integration for b^{clad} in Eq. (8) is performed within the lightcone in the cladding (e.g., for $\kappa \leqslant \tilde{\omega} n_c$). As shown above, both $R^s(\kappa)$ and $R^p(\kappa)$ are close to the corresponding $R^s_{\mathrm{eff}}(\kappa)$ and $R^p_{\mathrm{eff}}(\kappa)$ in this range. Hence, it is expected that $b^{\mathrm{clad}}_{\mathrm{HMMm}} \approx b^{\mathrm{clad}}_{\mathrm{HMMd}} \approx b^{\mathrm{clad}}_{\mathrm{eff}} \approx b^{\mathrm{clad}}_m$, which was confirmed in numerical calculations.

Furthermore, Eq. (4) ensures that $e^{2iw_c h} = e^{-2q_c h}$ decays exponentially for large κ. This introduces a cutoff in the integrand of $b_>$ in Eq. (15), and in the case of the effective medium where $\mathrm{Im}R^p_{\mathrm{eff}}(\kappa \to \infty) = \mathrm{const.}$, this is what makes an otherwise infinite integral in that term finite. This cutoff is heavily dependent on h: the smaller h, the larger the range of κ that significantly contribute. This range can be quantified by introducing $\kappa_{\mathrm{dipole}}(h)$ defined so that the contribution to b in Eq. (12) for all $\kappa \leqslant \kappa_{\mathrm{dipole}}$ is 90% of the total b. If h is significantly small, it can be expected that κ_{dipole} is large, so $b_>$ should be the dominant contribution to b in Eq. (13). Taking into account that, for κ significantly exceeding κ_{cr}, we can assume $\mathrm{Im}R^s(\kappa) \ll \mathrm{Im}R^p(\kappa) \approx \mathrm{Im}R^p_{\mathrm{eff}}(\kappa \to \infty)$ and $q_c \approx \kappa$, we can determine κ_{dipole} from Eq. (15) by solving

$$\frac{\int_{\kappa_{\mathrm{dipole}}}^{\infty} \kappa^2 e^{-2\kappa h} d\kappa}{\int_{\kappa_{\mathrm{cr}}}^{\infty} \kappa^2 e^{-2\kappa h} d\kappa} = 0.1, \tag{46}$$

resulting in

$$\frac{e^{-2h\kappa_{\mathrm{dipole}}}[1 + 2h\kappa_{\mathrm{dipole}}(1 + h\kappa_{\mathrm{dipole}})]}{e^{-2h\kappa_{\mathrm{cr}}}[1 + 2h\kappa_{\mathrm{cr}}(1 + h\kappa_{\mathrm{cr}})]} = 0.1. \tag{47}$$

In the limits of $\kappa_{\mathrm{dipole}} \gg \kappa_{\mathrm{cr}}$ and $h\kappa_{\mathrm{cr}} \ll 1$, Eq. (47) can be solved numerically, yielding a universal condition for an HMM:

$$h\kappa_{\mathrm{dipole}} \approx 2.661, \tag{48}$$

and confirming that κ_{dipole} is proportional to h^{-1} if h is small. For the chosen wavelength $\lambda = 715$ nm, Eq. (48) results in $\kappa_{\mathrm{dipole}}/\tilde{\omega} = (303\ \mathrm{nm})h^{-1}$; calculations show that this approximation is good for $h \leqslant 25$ nm.

Decreasing h will enhance the coupling between the emitter and any medium, so if the medium is absorbing (i.e., a bulk metal), decreasing h will also lead to an increase of b. This is a known quenching effect caused by coupling between the dipole's evanescent field and evanescent waves in the metal. Such quenching will also happen in the HMM because real HMMs include metallic layers and because the effective medium behaves like a metal for certain field components. However, when the medium supports propagating high-κ modes (either as a homogeneous effective medium or as a multilayer), $\mathrm{Im}R^p_{\mathrm{eff}} \gg \mathrm{Im}R^p_m$ for $\kappa > \kappa_{\mathrm{cr}}$ (see Figs. 5 and 6), and the increase in b is expected to be much stronger near HMMs than near metals. As we can now confirm, it is through this mechanism that the HMM modes and the associated increase of the photonic DOS give rise to the spontaneous emission enhancement known as the broadband Purcell effect and reported in previous theoretical and experimental works [7,11].

Note that the high-κ modes are essentially propagating; absorption in the metal just introduces a decay constant (so that these modes do eventually get absorbed) but does not make them truly evanescent. Hence the associated spontaneous emission enhancement is relatively insensitive to the absorption losses. This is in stark contrast to coupling between a dipole and resonant excitations such as surface plasmons, where the width of the resonance, and hence the strength of the effect, would depend heavily on the amount of absorption in the system.

We can see that the Purcell enhancement factor will be the same for the real HMM and for the effective medium if (and only if) $\mathrm{Im}R^p_{\mathrm{eff}}$ and $\mathrm{Im}R^p_{\mathrm{HMM}\mathbf{m},\mathbf{d}}$ are in good agreement all the way up to the cutoff $\kappa_{\mathrm{dipole}}(h)$ in the integrand of Eq. (15). According to Eq. (39), $\mathrm{Im}R^p_{\mathrm{HMM}\mathbf{m},\mathbf{d}}$ breaks away from $\mathrm{Im}R^p_{\mathrm{eff}}$ for larger κ if d [the average layer thickness as defined in Eq. (5)] is smaller (see Fig. 5). Therefore, for any given d, the effective-medium approach will correctly predict the dipole radiation rate for larger h but will break down as h becomes smaller. Indeed, the example in Fig. 2 shows that $b_{\mathrm{HMM}\mathbf{m}}$ changes from following b_{eff} to following b_m, and $f_{\mathrm{HMM}\mathbf{m}}$ changes from following f_{eff} to approaching f_m as h decreases.

The applicability region of the effective-medium approach to describing the HMMs should thus be derived in terms of a relation between d and h. Where there is a good agreement between R^p and R^p_{eff} (i.e., for filling fractions greater than around 0.25 as seen in Fig. 9), we should compare κ_{dipole} with κ_{upper} as obtained from Eq. (36), and assume that the agreement is good enough if

$$\kappa_{\mathrm{dipole}} < \kappa_{\mathrm{upper}}/2. \tag{49}$$

The case $\rho = 0.5$ is special because κ_{upper} can be determined analytically from Eq. (39), and because κ_{upper} for any other filling fraction is greater [see Fig. 7(b)], so Eq. (49) with $\rho = 0.5$ can be used as an over-restrictive effective-medium applicability condition for other filling fractions. For the chosen values of ϵ_m and ϵ_d, it results in a criterion $d < h/6.5$.

However, for the values of ρ that approach ρ_1, the correspondence between R^p and R^p_{eff} is poor due to the influence of the topmost layer (see Figs. 9 and 6). Then, κ_{dipole} should be compared to κ_{sp} in Eq. (42) instead:

$$\kappa_{\mathrm{dipole}} \ll \kappa_{sp}, \tag{50}$$

resulting in a different, far stronger criterion, $d \ll h/11$, for the chosen values of ϵ_m and ϵ_d.

For large h, the field reaching the multilayer no longer couples to the high-κ HMM modes ($\kappa_{\mathrm{dipole}} < \kappa_{\mathrm{cr}}$), and the applicability condition for the effective-medium approach eventually becomes the usual subwavelength criterion, as modified by the large $|\epsilon|$ in the materials involved ("strongly subwavelength" in vacuum means $d \ll 715$ nm, while "strongly subwavelength" in bulk gold requires $d \ll 170$ nm).

To illustrate the obtained applicability conditions, we calculate b for the structures with $\rho = 0.5$ as in Ref. [7] and show the results in Fig. 10. At $h = 100$ nm, which is still subwavelength in the cladding but much larger than d, we see that $b_{\mathrm{HMM}} > b_m \gtrsim b_d$ [Fig. 10(a)]. The results for the real HMM converge to those for the effective medium as $d \to 0$; for HMM**m**, $b < b_{\mathrm{eff}}$, so, in accordance with Fig. 2, the structure's properties tend toward those of a bulk metal

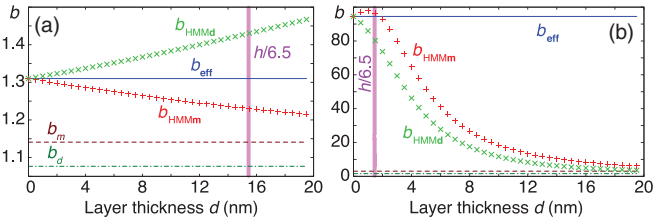

FIG. 10. (Color online) Total radiation rate b for varying d for a dipole placed at (a) $h = 100$ nm and (b) $h = 10$ nm from the surface of an HMM with $\rho = 0.5$. Horizontal lines correspond to the values for the effective medium (b_{eff}), bulk metal (b_m), and bulk dielectric (b_d). The vertical line corresponds to the value of d according to the criterion in Eq. (49).

as d increases. For HMM**d**, the trend is opposite, which is associated with an increase in photonic DOS as the structure gets closer to being a photonic multilayer in the "transparent metal" regime [35]. The effective-medium approach is seen to predict the qualitative behavior of the HMM within 10% accuracy if, following Eq. (49), $d < h/6.5 \simeq 15.3$ nm.

For the deeply subwavelength, near-field regime ($h = 10$ nm), one can see that $b_{\mathrm{HMM}} \gg b_{m,d}$ [Fig. 10(b)], in agreement with predictions in earlier work [7–9,11]. However, in spite of the subwavelength layer thicknesses, the effective-medium approach largely fails to predict the correct values of b unless $d \ll h$, namely, $d < h/6.5 \simeq 1.5$ nm, again following Eq. (49).

This situation changes drastically for the structures with a different filling fraction $\rho = 0.156$, as seen in Fig. 11. We still see convergence toward b_{eff} as $d \to 0$ but it is more complicated. In particular, for $h = 10$ nm there is a region of layer thicknesses where $b_{\mathrm{HMM}\mathbf{m}}$ significantly exceeds b_{eff} because of the overshoot in $\mathrm{Im}R^p$ due to SRSPP excitation in the topmost metal layer. For $d = 1.5$ nm, the differences still exceed 30%, and no decent agreement is seen until $d \lesssim 0.2(h/11)$ in accordance with the condition (50). For $h = 100$ nm, the overshoot effects play a weaker role, so the convergence remains within 12% up to $d = 15$ nm.

Finally, for the fraction of radiation going into the cladding (Fig. 12) we see that $f_{\mathrm{HMM}} \ll f_{m,d}$ if h and d are both sufficiently small, in agreement with earlier predictions [7–9,11]. However, the effective-medium approach again fails to predict the correct values of f unless $d \ll h$. For values of $d \sim 10$–20 nm, the effective-medium approach greatly overestimates the HMM performance compared to the real structure, yielding b_{eff} 5–10 times greater than the actual b and f_{eff} 10–15 times smaller than the actual f [16]. Equation (49)

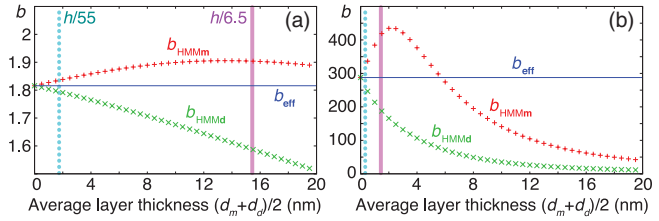

FIG. 11. (Color online) Same as Fig. 10 but for $\rho = 0.156$. Solid and dotted vertical lines denote the values of d corresponding to the criteria in Eqs. (49) and (50), respectively.

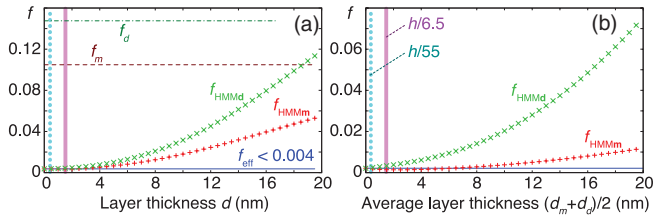

FIG. 12. (Color online) Fraction of radiation $f = b^{\text{clad}}/b$ from a dipole located $h = 10$ nm from a semi-infinite HMM, directed into the cladding for (a) $\rho = 0.5$ and (b) $\rho = 0.156$.

seems to be an applicable validity condition. For smaller values of filling fraction, the SRSPP-mediated overshoot effects result in a region where $f_{\text{HMMm}} < f_{\text{eff}}$ so the range where the effective-medium approach is good enough for practical purposes is extended.

We note finally that the SPP excitations in the topmost metallic layer can be controlled independently of bulk propagating waves in the HMM by making the topmost layer of different thickness than the rest of metallic layers in the HMM. This can be used to maximize the performance of a particular multilayer HMM, as well as to tailor it to the properties of a particular emitter.

V. CONCLUSIONS

In summary, we have explored the optical properties of multilayered hyperbolic metamaterials (HMMs) by investigating the behavior of the Fresnel reflection coefficients at the boundary between the metamaterial and the ambient medium. We have shown how a band of bulk propagating modes, located far outside the lightcone of any isotropic medium, is formed in metal-dielectric multilayer HMMs, and how these modes become large-wave-vector propagating modes in homogeneous indefinite media. It is shown how modes from this band interact with evanescent field of an emitter placed in close proximity, giving rise to exotic behavior of HMMs previously reported [7–9,11], including the broadband Purcell effect [7] and suppressed outward scattering [9].

Conditions for the applicability of the effective-medium approximation can be formulated in the form of Eqs. (49) and (50). They relate the thickness of the metal layer (d_m) and the dielectric layer (d_d) in the HMM to the distance h between the emitter and the HMM surface. For most values of the metal filling fraction $\rho = d_m/(d_m + d_d) \in [\rho_1, \rho_2]$ where ρ_1 and ρ_2 are defined by $\text{Re}[\rho_1\epsilon_m + (1-\rho_1)\epsilon_d] = 0$ and $\text{Re}[\rho_2\epsilon_m^{-1} + (1-\rho_2)\epsilon_d^{-1}] = 0$ and denote the region where the multilayer has hyperbolic dispersion [see Eqs. (16)–(18)], the relation can be expressed as

$$\frac{d_m + d_d}{h} < \frac{1}{5.32}\text{Re}\ln\left[2\frac{(\epsilon_m - \epsilon_d)^2 - 4\epsilon_m\epsilon_d}{(\epsilon_m + \epsilon_d)^2}\right], \quad (51)$$

where ϵ_m and ϵ_d are permittivities of metal and dielectric, respectively. For $\rho_1 < \rho < 0.25$, the condition is stricter:

$$\frac{d_m}{h} \ll \frac{1}{2.66}\text{Re}\ln\left[\frac{\epsilon_m - \epsilon_c}{\epsilon_m + \epsilon_c}\right], \quad (52)$$

where ϵ_c is the dielectric constant of the cladding.

These relations are seen to depend on the metamaterial design and are very different from conventional assumptions about subwavelength layer thicknesses. Overall, the effective-medium approach has a rather poor accuracy for the layer thicknesses used in reported experiments. Usually, it overestimates the effect of a multilayer HMMs unless the layer thicknesses are brought down to a few nanometers. However, with the values of the metal filling fraction close to ρ_1 in Eq. (18), a multilayer HMM can outperform the corresponding homogenized medium. This is explained by an additional coupling between large-wave-vector modes and the dipole field through intermediate excitation of short-range surface plasmon polaritons in the outermost layer of the metamaterial.

The results obtained can be straightforwardly generalized to multilayer structures of a more complex composition. In addition, extension of results to the case of a dipole inside an HMM would be intriguing [17,18].

ACKNOWLEDGMENTS

The authors thank M. Liscidini for helpful suggestions. This work was supported by the Natural Sciences and Engineering Research Council of Canada (NSERC).

[1] J. Pendry, Opt. Express **11**, 639 (2003).
[2] M. Kuwata-Gonokami, N. Saito, Y. Ino, M. Kauranen, K. Jefimovs, T. Vallius, J. Turunen, and Y. Svirko, Phys. Rev. Lett. **95**, 227401 (2005).
[3] D. R. Smith, D. Schurig, J. J. Mock, P. Kolinko, and P. Rye, Appl. Phys. Lett. **84**, 2244 (2004).
[4] D. R. Smith, D. Schurig, and P. Kolinko, J. Opt. Soc. Am. B **21**, 1032 (2004).
[5] A. Degiron, D. R. Smith, J. J. Mock, B. J. Justice, and J. Gollub, Appl. Phys. A **87**, 321 (2007).
[6] W. Yan, L. Shen, L. Ran, and J. A. Kong, J. Soc. Am. A **24**, 530 (2007).
[7] Z. Jacob, J.-Y. Kim, G. V. Naik, A. Boltasseva, E. E. Narimanov, and V. M. Shalaev, Appl. Phys. B **100**, 215 (2010).
[8] I. I. Smolyaninov and E. E. Narimanov, Phys. Rev. Lett. **105**, 067402 (2010).
[9] E. Narimanov, M. A. Noginov, H. Li, and Y. Barnakov, in *QELS Conference: OSA Technical Digest 2010* (CD), Optical Society of America, paper QPDA6.
[10] M. A. Noginov, Yu. A. Barnakov, G. Zhu, T. Tumkur, H. Li, and E. E. Narimanov, Appl. Phys. Lett. **94**, 151105 (2009).
[11] M. A. Noginov, H. Li, Yu. A. Barnakov, D. Dryden, G. Nataraj, G. Zhu, C. E. Bonner, M. Mayy, Z. Jacob, and E. E. Narimanov, Opt. Lett. **35**, 1863 (2010).
[12] X. Ni, G. Naik, A. Kildishev, Yu. Barnakov, A. Boltasseva, and V. Shalaev, Appl. Phys. B **103**, 553 (2011).
[13] M. A. Noginov, Yu. A. Barnakov, G. Zhu, T. Tumkur, H. Li, and E. E. Narimanov, Appl. Phys. Lett. **94**, 151105 (2009).

[14] J. Kanungo and J. Schilling, Appl. Phys. Lett. **97**, 021903 (2010).
[15] A. Fang, T. Koschny, and C. M. Soukoulis, Phys. Rev. B **79**, 245127 (2009).
[16] O. Kidwai, S. V. Zhukovsky, and J. E. Sipe, Opt. Lett. **36**, 2530 (2011).
[17] I. Iorsh, A. Poddubny, A. Orlov, P. Belov, and Yu. S. Kivshar, Phys. Lett. A **376**, 185 (2012).
[18] A. N. Poddubny, P. A. Belov, and Yu. S. Kivshar, Phys. Rev. A **84**, 023807 (2011).
[19] R. Kotyński, T. J. Antosiewicz, K. Król, and K. Panajotov, J. Opt. Soc. Am. A **28**, 111 (2011).
[20] R. Kotyński, T. Stefaniuk, and A. Pastuszczak, Appl. Phys. A **103**, 905 (2011).
[21] R. Kotyński, Opto-Electronics Rev. **18**, 366 (2010).
[22] J. E. Sipe, Surf. Sci. **105**, 489 (1981).
[23] J. J. Saarinen and J. E. Sipe, J. Mod. Opt. **55**, 13 (2008).
[24] M. Born and E. Wolf, *Principles of Optics*, 6th ed. (Cambridge University Press, Cambridge, UK, 1997).
[25] J. M. Wylie and J. E. Sipe, Phys. Rev. A **32**, 2030 (1985).
[26] A. Yariv and P. Yeh, *Optical Waves in Crystals* (Wiley, New York, 1983).
[27] P. G. Etchegoin, E. C. Le Ru, and M. Meyer, J. Chem. Phys. **125**, 164705 (2006).
[28] T. S. Eriksson, A. Hjortsberg, G. A. Niklasson, and C. G. Granqvist, Appl. Opt. **20**, 2742 (1981).
[29] S. Feng, J. M. Elson, and P. L. Overfelt, Opt. Express **13**, 4113 (2005).
[30] G. Rosenblatt and M. Orenstein, Opt. Express **19**, 20372 (2011).
[31] J. Sun, Ji Zhou, Bo Li, and F. Kang, Appl. Phys. Lett. **98**, 101901 (2011).
[32] S. V. Zhukovsky, Phys. Rev. A **81**, 053808 (2010).
[33] P. Berini, Adv. Opt. Photon. **1**, 484 (2009).
[34] J. Saarinen, S. Weiss, P. Fauchet, and J. E. Sipe, Opt. Express **13**, 3754 (2005).
[35] M. J. Bloemer and M. Scalora, Appl. Phys. Lett. **72**, 1676 (1998).